IEEE Access
Multidisciplinary | Rapid Review | Open Access Journal

Received May 28, 2021, accepted July 9, 2021, date of publication July 15, 2021, date of current version July 26, 2021.

Digital Object Identifier 10.1109/ACCESS.2021.3097382

Instrument Design for Detecting the Inner Damage of Casing

TAO GUO[1], YONG WEI[1], KE LI[2], QIANG CHEN[2], LI YAN[3], AND JIEFU CHEN[1,3], (Senior Member, IEEE)

[1]School of Electronics and Information, Yangtze University, Jingzhou 434023, China
[2]Equipment and Sales Branch, China Petroleum Logging Company Ltd., Xi'an 710077, China
[3]Department of Electrical and Computer Engineering, University of Houston, Houston, TX 77044, USA

Corresponding authors: Yong Wei (weiyong@yangtzeu.edu.cn) and Jiefu Chen (jchen82@central.uh.edu)

This work was supported in part by the China Petroleum Science and Technology Innovation Fund under Grant 2017D-5007-0306, and in part by the China Major Science and Technology Project under Grant 2017ZX05019001.

ABSTRACT Detecting and localizing the inner damage of the downhole casing is crucial for oil and gas production. The current methods for damage detection suffer from polarization effect, capacitance effect, and difficulty in measuring weak direct current signals. As an alternative, we propose a new instrument design based on a six-electrode array in this study. The basic detection principle is introduced, and the key factors that affect the detection performance are studied through modeling and simulation. Besides, the entire system of the instrument design consisting of several modules is presented. In addition, an experiment is conducted to demonstrate the detection capability of the proposed design. It is found that the detection dynamic of the instrument is 93 dB and a signal-to-noise ratio is 73 dB. It can detect damage when salinity is lower than 120 g/l and can identify the location of damage with high resolution in the longitudinal and radial directions.

INDEX TERMS Instrument design, damage detection, damage localization, six-electrode array.

I. INTRODUCTION

Changqing Oilfield located in northwest China has high underground mineralization, and the resulting electrochemical effects cause the casing wall corrosion to be extremely serious. For this reason, petroleum engineers have taken protective measures, by using an epoxy cold package with sacrificial anodes above the liquid level, and applying coating made of DPC (a phenolic resin) below the liquid level and in the production layer [1]–[5]. However, the deformation of the downhole casing can easily lead to the peeling of the inner casing coating, and the physical scraping between the instrument and the borehole wall will also cause the damage of the inner casing coating, resulting in the decrease of the anti-corrosion effect of the inner casing coating [6]. As a consequence, the normal production of oil and gas and the downhole operation are severely affected, Therefore, it is of great significance to inspect the inner casing coating [7].

At present, the methods used to detect casing coating damage mainly include downhole electromagnetic thickness measurement, multi-arm caliper, optical television imaging, ultrasonic imaging, and related electrical logging technologies. Downhole electromagnetic thickness measurement technology can not produce electromagnetic signal feedback on thin coating [8]; Multi-arm caliper logging tool can detect the change of inner diameter of oil casing, but it can not detect the quality of coating, and the attachments on oil casings will affect the measurement accuracy [9]; Optical imaging logging technology is affected by the surface cleanliness and limited space perspective of downhole oil casing, so it is difficult to accurately judge the specific situation of the inner coating of oil casing; Although the ultrasonic imaging logging tool can be applied to casing quality evaluation, its eccentricity has a great influence on the measured value, and it has not been used to detect the damage of inner coating [10]. Electric logging technology can be divided into single electrode method, multi-electrode method, and micro-electrode methods according to the measurement methods used. The single-electrode method can reflect the overall quality of the casing inner coating, but it can not detect local damages [11]. Most of the multi-electrode methods use the DC current detection method, which can not solve the polarization effects caused by electrolyte [12], [13]; The microelectrode method requires the instrument to be close to the inner wall of the casing, which can effectively detect the local coating quality, but it is easy to miss the area where the casing does not contact

The associate editor coordinating the review of this manuscript and approving it for publication was Datong Liu.

with the coating [14]. In 2011, Wan *et al.* proposed the Field Signature Method [15]. It was easy to explain and imagine. However, this detection method can not locate defects in the thickness direction and it is difficult to detect DC signals [16]. To meet the overall detection requirements of casing inner coating, a method based on conductivity characteristics was proposed, and the key factors affecting the measurement performance were analyzed. Moreover, an instrument design based on the six-electrode array was developed and tested with field experiments.

The rest of the paper is organized as follows. In Section 2, the detection method of conductivity is analyzed, the detection model is established, and the best detection parameters are analyzed. In Section 3, the instrument scheme is given, and in Section 4 and Section 5, the results and analysis of indoor and outdoor experiments are given.

II. DETECTION PRINCIPLE AND SCHEME OF CASING INNER COATING

A. DETECTION PRINCIPLE

The coating material used in DPC inner coating anti-corrosion technology of casing is phenolic resin, which is a typical insulating material [17], [18]. Therefore, when the quality of the coating in the casing decreases or is damaged, the conductivity between the casing and the well fluid near the damaged location will increase sharply [19]. According to this feature, if a detection electrode is placed close to the damaged part in the well fluid and an excitation voltage source is applied between the casing opening and the detection electrode, the damaged part of the casing can be regarded as a metal electrode, and the current between the damaged part of the casing and the detection electrode can indirectly reflect the damage degree of the coating. The detection schematic diagram is shown in Fig. 1(a). In order to detect the current, a sampling resistor R_s is connected in series in the current loop, and the current in the loop can be detected by collecting the voltage difference between the two ends of the sampling resistor R_s. In other words, when the damaged area S of the inner coating increases, it means that the smaller the resistance R_x between AB points, the larger the loop current I will be, and the larger the voltage U obtained on the sampling resistance will be [20]. There is the following relationship between them: Coating damage $S\uparrow\rightarrow R_x\downarrow\rightarrow I\uparrow\rightarrow V_s\uparrow$; On the contrary, the coating is damaged $S\downarrow\rightarrow R_x\uparrow\rightarrow I\downarrow\rightarrow V_s\downarrow$. Therefore, by detecting the change of sampling voltage V_s, the loop current can be reflected, and the damage of casing inner coating can be measured indirectly. Considering that minerals widely existing in drilling fluid are easy to produce polarization effect, AC signal should be used as excitation signal for voltage source. The detection circuit can be equivalent to the model shown in Fig. 1(b) [21], [22].

R_x in Fig. 1 is the solution resistance of the two electrodes, which is related to the exposed the area of electrode plate and the salinity of the well fluid, and is a physical quantity that we need to measure. C_x is the capacitance produced by the electric double layer effect, which is greatly affected by the

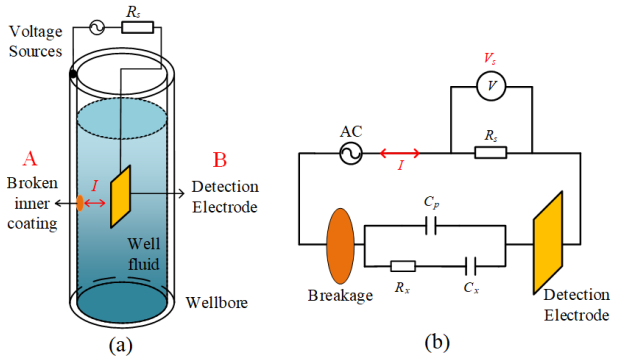

FIGURE 1. Conductivity-based damage detection method for inner casing coating. (a) Detection schematic; (b)Equivalent impedance detection model.

concentration of well fluid electrolyte, and its size is generally tens or even hundreds of μf; C_p is the distributed capacitance caused by the distribution of electrode wires, which is related to the length of electrode wires, and its order of magnitude is usually pf [23]. According to the equivalent circuit model of the sensor, the equivalent circuit impedance model is:

$$Z = (R_x + \frac{1}{j\omega C_x})||\frac{1}{j\omega C_p} \tag{1}$$

As we all know, the capacitive reactance of a capacitor is inversely proportional to the capacitance value and the angular frequency ω. Therefore, when the conductivity is measured by the electrode method, the higher excitation signal frequency is beneficial to reduce the influence of the polarization effect, but at the same time, the capacitive reactance of the distributed capacitance C_p will be reduced, which will lead to the increase of branch current flowing through the well. The current of the liquid resistor R_x decreases, which easily causes measurement errors. Therefore, the measurement frequency of AC impedance is generally in the order of 10^3 Hz to 10^4 Hz [24]. Generally, the impedance of double-layer capacitance C_x and lead distributed capacitance C_p will affect the measurement results, and the size of C_x can often reach more than 1000 times of C_p. According to the calculation formula of capacitive reactance, when an AC signal with a frequency of 1KHz is used as an excitation source, it is assumed that the capacitance of C_x is 100 μF and that of C_p is 10pF. Using the capacitive reactance calculation formula, it can be known that the capacitance reactance of C_x will not exceed 1.6Ω, while the capacitive reactance of C_p is about 15.9MΩ, and the impedance value of C_x is far less than that of distributed capacitor C_p. However, the well fluid resistance R_x is affected by the limited space volume and salinity in the well, and its resistance is generally in the range of several hundred to several thousand ohms. Therefore, the influence of C_x on the measurement results can be neglected, and the equivalent impedance Z between the damaged part and the electrode is simplified as:

$$Z = \frac{R_x \cdot (1 - j\omega R_x C_p)}{1 + {R_x}^2 j^2 \omega^2 {C_p}^2} \tag{2}$$

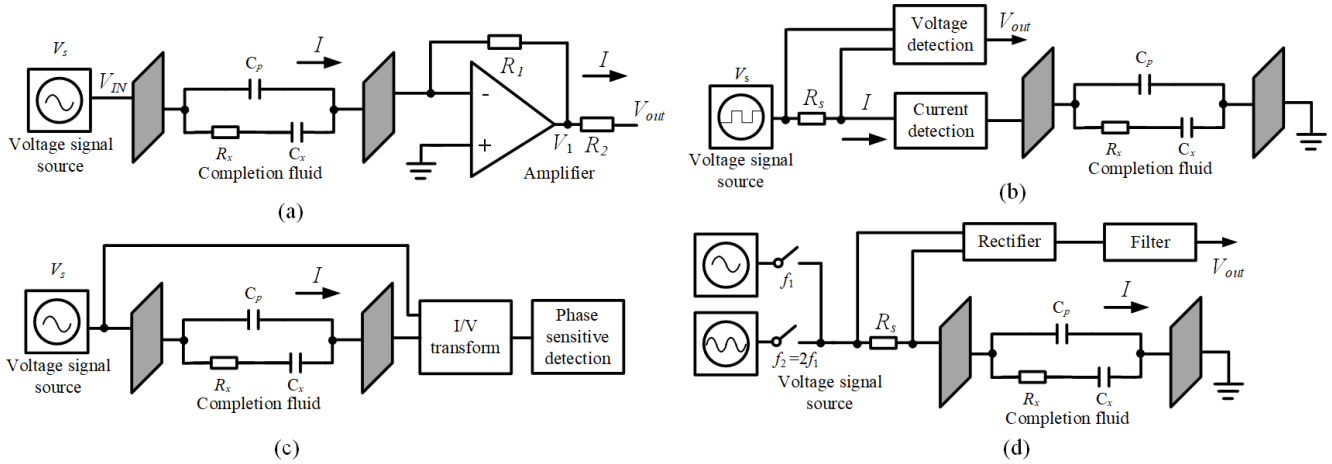

FIGURE 2. Conductivity test method: (a) Operational amplifier conductivity measurement method; (b) Bipolar pulse excitation method; (c) Phase-sensitive measurement method; (d) Dual-frequency sinusoidal signal measurement method.

It can be seen from equation (2) that when the value of $j\omega C_p$ is close to 0, the impedance Z obtained by measuring the conductivity by the DC electrode method is equal to the well fluid resistance R_x. If the well fluid impedance between the two electrodes is measured directly, the actual measured value will be the complex impedance value of the well fluid instead of the well fluid resistance, which will lead to great measurement error [25].

B. CONDUCTIVITY MEASUREMENT METHOD

To accurately measure the actual well fluid resistance and solve the influence of capacitance effect and polarization effect on the measurement results, we have studied several mature conductivity measurement methods at present: operational amplifier conductivity measurement method [26], bipolar pulse excitation method [27], phase-sensitive detection method [28] and dual-frequency sinusoidal signal measurement method [29], These methods have their advantages in reducing measurement errors.

The operational amplifier conductivity measurement method is shown in Fig. 2(a). By applying AC constant voltage signal to the solution to be measured and measuring the current passing through the sensor, the conductivity of the solution can be indirectly obtained. The advantage of this method is that the output voltage of the operational amplifier has a linear relationship with the conductivity of the measured solution within the measuring range, which solves the problem of non-linear change of the measured resistance value and the problem of sensor resolution reduction when the conductivity of the solution is large. However, in the practical design of an operational amplifier circuit, it is necessary to carefully consider the impedance change caused by AC signal to a double-layer capacitor, as well as the factors such as open-loop gain, input impedance, passband bandwidth, power supply influence, and quality factor of an operational amplifier, which makes the implementation more complicated.

As shown in Fig. 2(b), the bipolar pulse excitation method can effectively eliminate the influence of electric double-layer capacitance on the measurement of solution resistance. The basic idea is to use a bipolar square wave signal to charge and discharge the electric double layer capacitor C_x repeatedly, so when the capacitor charge and discharge reach steady-state, C_x is equivalent to a short circuit state. According to Kirchhoff's voltage law, at this time, only the sampling resistor R_s and the solution resistor R_x are in the circuit for voltage division, and the solution resistance can be calculated after collecting and processing the voltage difference between both ends of R_s. Although the bipolar pulse measurement method can eliminate the influence of the capacitance effect in principle, it has high requirements on the conversion speed and detection accuracy of the detection circuit. Considering that the potential difference and spontaneous potential between the earth and the ground of the power supply will interfere with the detection process, the bipolar pulse signal needs to strictly keep 50% duty cycle in the detection process to achieve better detection results. Otherwise, the pulse edge can not be accurately judged, and the voltage at both ends of the sampling resistor Rs can not be differentially sampled at the appropriate time point. Therefore, it is considered that this method has high requirements for the detection environment and is difficult to be practically applied to the measurement of well fluid conductivity.

Fig. 2(c) is the basic principle diagram of the phase-sensitive measurement method. Its basic idea is to realize accurate resistance measurement by collecting the phase difference and amplitude difference between the excitation end and the detection end of the sinusoidal excitation signal. Because the resistance has no phase shift effect on the current phase, the real part and imaginary part of the impedance can be separated [30]. Then, Discrete Fourier Transform (DFT) is used to calculate the voltage and current signals, and the amplitude-frequency characteristics and phase-frequency characteristics of sinusoidal signals are obtained. Then,

the impedance angle of the measured impedance is calculated to obtain the actual well fluid impedance. Although this method can improve the measurement accuracy of the resistance to be measured and eliminate the effects of polarization and capacitance effects, it is necessary to ensure that the phase difference between the sinusoidal signal of the measured resistance and the sinusoidal signals of other impedances is controlled at 90° during the measurement process. Otherwise, the influence of electric double-layer capacitance can not be completely filtered out, so this method is not suitable for the measurement of well fluid impedance.

The dual-frequency sinusoidal signal measurement method is shown in Fig. 2(d). Under the action of a sinusoidal signal with an excitation frequency of $\omega = 2\pi f$, the impedance of well fluid was measured twice, and the influence of the capacitance effect is eliminated through theoretical calculation. The calculation method is to calculate the equivalent circuit model in Fig. 1(b) by using the relevant formula of admittance. The RC parallel admittance in formula (2) is:

$$Y = \frac{1}{R_x} + j\omega C_p \tag{3}$$

The modulus of admittance is:

$$|Y| = \frac{1}{|Z|} = \frac{\sqrt{1 + (\omega C_p R_x)^2}}{R_x} \tag{4}$$

$|Z|$ is the module of impedance measured at this excitation frequency, and its value includes the influence of R_x and C_p. When the frequency of the excitation signal is 2ω, the measured impedance mode is:

$$\left|Z'\right| = \frac{R_x}{\sqrt{1 + 4\omega^2 {C_p}^2 {R_x}^2}} \tag{5}$$

Combine formula (4) and formula (5) for simultaneous solution, Make $t = \omega^2 {C_p}^2 {R_x}^2$:

$$t = \frac{\left|Z'\right|^2 - |Z|^2}{4|Z'|^2 - |Z|^2} \tag{6}$$

Combinations of formula (5) and formula (6) are available:

$$R_x = |Z|\sqrt{1 + t} \tag{7}$$

It can be seen from formula (6) and formula (7) that the dual-frequency sinusoidal signal measurement method only needs to measure the impedance values at different excitation frequencies. Substituting into the formula calculation can eliminate the influence of capacitance effect and polarization effect on an impedance measurement in principle. From the perspective of engineering realization, only two sinusoidal signals of different frequencies are used as excitation sources and the effective value of the voltage difference between the two ends of the sampling resistor is calculated and the real well fluid resistance can be obtained by substituting it into formula (7). In summary, we choose the dual-frequency sinusoidal signal measurement method and realize the accurate measurement of the real resistance of the well fluid [31].

C. KEY PROBLEMS OF CONDUCTIVITY DETECTION

In the practical application process of the casing inner coating quality inspection instrument, the damaged part of the casing inner coating is equivalent to one end of the detection electrode, and the other end of the detection electrode is placed on the instrument frame, which is used as two detection electrodes for conductivity inspection. According to the calculation formula for measuring solution resistance with parallel electrodes:

$$R_x = \frac{1}{G} = \frac{L}{S \cdot \sigma} = \sigma \frac{1}{K} \tag{8}$$

In the formula: K is electrode constant; σ is conductivity (S/cm); L is electrode spacing (cm); S is Detection electrode area (cm^2).

The electrode constant K of the conductivity sensor accurately describes the geometric characteristics of the two electrodes of the sensor. It is the length ratio of the sample in the key area between the two detection electrodes, which directly affects the sensitivity and accuracy of measurement. In the process of using a traditional conductivity cell to detect the conductivity of the solution, the determination of the conductivity cell constant and the cell constant has a great influence on the error in the detection process [32]. In order to accurately measure the conductivity of the well fluid, it is necessary not only to calibrate the conductivity cell constant with an accurate KCl solution but also to place a detection electrode with an accurate size to ensure that the detection electrode is in complete contact with the solution to be measured, thereby obtaining an accurate conductivity value [33], [34]. However, in the actual logging process, because of the complex electrolyte composition in the well fluid, the problem of dynamic liquid level, and the interference of various electromagnetic noises in the well, it is impossible to quantitatively determine the values of conductivity cell constant and electrode constant [35]. What we are more concerned about is whether a significant change in conductance can be observed on the detection electrode when the damaged area of the casing inner coating changes, so as to determine the relationship between the two and solve the practical engineering needs. To sum up, the key problems that need to be solved are:

(1) The structure and size of electrodes are very important in the measurement of conductivity. In order to design a reasonable electrode, it is necessary to analyze the influence of its structure and size on conductivity measurement and to provide a theoretical basis for selecting appropriate electrode parameters.

(2) During the detection process, an AC signal should be applied between the metal casing and the detection electrode, so as to ensure that the current flow through the well fluid as much as possible to form a loop between the two. Therefore, it is important to carefully isolate the signal source to reduce current dissipation.

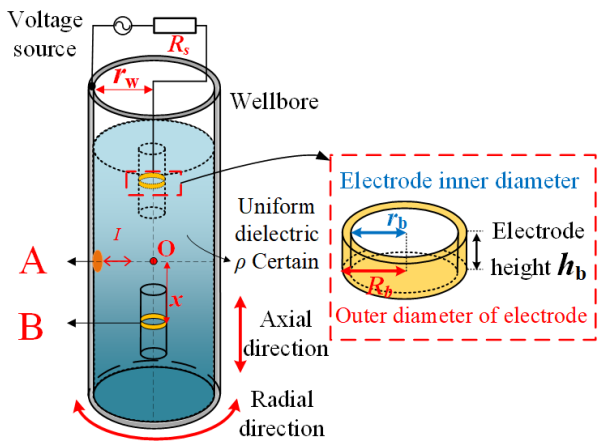

FIGURE 3. Schematic diagram of ring electrode detection model.

D. MODELING AND SIMULATION

According to the detection principle, and according to actual engineering needs, the detection model shown in Fig. 3 is proposed. Assuming that the inner radius of the wellbore whose inner surface is sprayed with the insulating coating on the inner surface is r_w, the interior is filled with a uniform medium with a conductivity of σ. There is circular damage with radius r_a on the surface of the inner coating of the wellbore. It is assumed that a cylindrical coordinate system is established at the intersection of the radial direction of the damage and the shaft axis of the wellbore, and O is the origin of the coordinate system. Place a ring-shaped detection electrode at the shaft center position B of the wellbore, the inner radius is r_b, the outer radius is R_b, the electrode height is h_b, and the distance between B and O is x. An AC voltage source is placed in the instrument. One end of the AC voltage source is connected with the upper edge of the metal casing located on the ground through a cable, and the other end is connected with the detection electrode. With the change of the depth of the detection electrode, the conductance between the detection electrode B and the damaged point will change correspondingly. By measuring the voltage on the sampling resistor, the area of the damaged position can be estimated and located indirectly.

According to the theory of electromagnetism, static charge produces an electrostatic field, and a steady current produces a steady current field. When the induced electric field is much smaller than the Coulomb electric field, a sinusoidal AC signal excitation can be used to obtain an electric quasi-static field. Use Maxwell's equations to solve the electric field inside the casing. The differential forms of the four equations are:

$$\begin{cases} \nabla \times H = J + \dfrac{\partial D}{\partial t} & \nabla \cdot B = 0 \\ \nabla \times E = -\dfrac{\partial B}{\partial t} & \nabla \cdot D = \rho \end{cases} \tag{9}$$

In the formula, B, D, E, H, J, V, ϵ, ρ, σ, μ are magnetic induction intensity, electric displacement, electric field intensity, magnetic field intensity, current density, electric potential, dielectric constant, charge density, electrical conductivity and magnetic permeability, respectively [36]. For time-varying electric fields and currents, when the magnetic effect is negligible, the basic equation of the differential form of the electrical quasi-static field is:

$$\begin{cases} \nabla \times H = J + \dfrac{\partial D}{\partial t} & \nabla \cdot B = 0 \\ \nabla \times E = 0 & \nabla \cdot D = \rho \end{cases} \tag{10}$$

Under the time-varying condition, the time-varying electric field is approximately irrotational, and the divergence of electric displacement D is still equal to the free charge density at that point. According to the current conservation equation:

$$\nabla \cdot J + \frac{\partial \rho}{\partial t} = 0 \tag{11}$$

Take the divergence of the differential form of the full current law formula in equation (10) to obtain the constant current equation:

$$\nabla \cdot J + \frac{\partial \nabla \cdot D}{\partial t} = 0 \tag{12}$$

The general medium is isotropic, and the physical property equation of its properties is:

$$J = \sigma ED = \varepsilon EB = \mu H \tag{13}$$

The basic boundary conditions of the electric quasi-static field include the conservation of current and Faraday's law, the differential form of which is:

$$\begin{cases} \nabla \cdot J = -\dfrac{\partial \rho}{\partial t} \\ \nabla \times E = 0 \end{cases} \tag{14}$$

According to the calculation formula of electric potential and electric field strength:

$$E = -\nabla V \tag{15}$$

Simulation of conduction current J_c and displacement current J_d in time-varying electric field:

$$\begin{cases} J_c = \sigma E \\ J_d = j\omega\varepsilon E \end{cases} \tag{16}$$

To sum up, we use equations (14), (15), and (16) to establish a quasi-static analysis model of an electric field in the casing. The established model satisfies the above-mentioned correlation equation internally, while the edge satisfies the relevant boundary conditions. Considering that COMSOL has a powerful simulation function [37]. We use this software to analyze the current loop and determine the parameters of the detection electrode.

Based on the conductivity detection model, the AC/DC module of the simulation tool and Dirichlet boundary conditions are selected to establish the casing detection model, and its key parameters are studied [38]. Because the bottom of the casing is in direct contact with the earth, the electric

TABLE 1. Model default parameter table.

Parameter	Value	Description
V_{ac}	10 V	Magnitude of voltage
R_b	0.04 m	Outer radius of electrode
r_b	38 cm	Inner radius of electrode
r_a	0.01 m	Radius of defect
r_w	0.07 m	Radius of well
σ	0.1ms/cm	Well fluid conductivity
h_b	0.01 m	Height of electrode
h_w	40 m	Height of well
d_d	0.1 m	Distance to defect

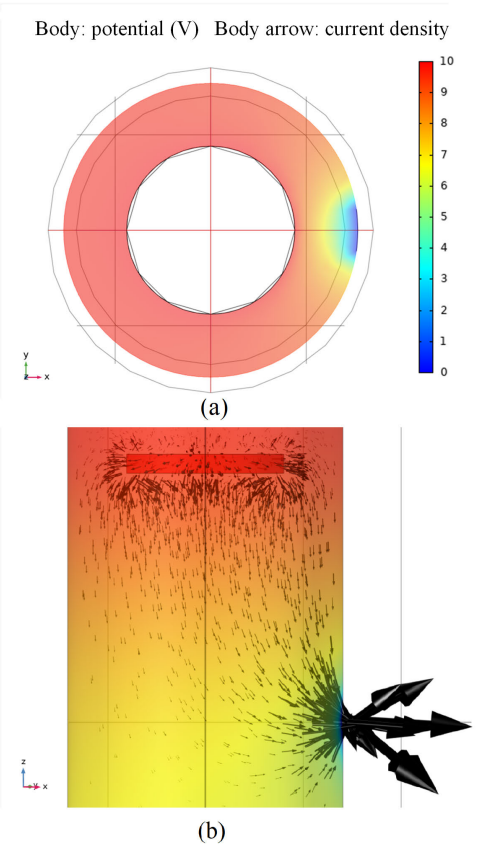

FIGURE 4. Schematic diagram of potential distribution in casing. (a) Top view; (b) Main view.

potential is set to 0 V; When the inner coating of the wellbore is intact, the inner wall of the wellbore is set to be electrically insulated. To reduce the number of grids and the amount of calculation, and speed up the simulation speed of the model, the impedance boundary condition is set to simulate a thin layer with high resistivity. The relevant default parameters used in the simulation model are shown in Table 1.

Circular damage appears on the insulating inner wall of the wellbore at a certain depth, and the electric potential distribution result at a certain moment is obtained by simulation calculation, as shown in Fig. 4. Simulation results show that: (1) The potential between the damaged part of the wellbore coating and the detection electrode shows a downward trend, the potential distribution in other areas is uniform, and the current direction is consistent with expectations; (2) The electric potential is attenuated by 38dB from the maximum value to the minimum value, which fully meets the resolution requirements from the perspective of detection; (3) To improve the degree of the current collection, reduce the escape of loop current through the earth and isolate other interference, it is recommended to take isolation measures in the excitation voltage source.

Because the conductivity of the well fluid and the damaged area of coating in a wellbore are unknown, it is necessary to optimize the size parameters of the detection electrode as much as possible to meet the measurement requirements of different well conditions. In general, we mainly consider (1) The influence law of well fluid salinity; (2) The relationship between the position, size, damaged area of the detection electrode, and the equivalent resistance of the well fluid. (3) Number selection and distribution scheme of detection electrodes. In order to determine the appropriate electrode parameters, the control variable method is used to simulate the sensitive variables, and the default values of Table 1 are selected for the remaining parameters.

1) THE INFLUENCE LAW OF WELL FLUID SALINITY

Because the salinity of the well fluid is different under different well conditions, it is required that the measuring range of the electrode be as wide as possible. Therefore, it is necessary to study the relationship between the radius r_a of the damaged area and the conductivity of the well fluid under different salinity conditions. Fig. 5(a) shows the simulation results under four different salinity conditions of well fluids. The results show that with the increase of salinity of well fluid, the current density increases obviously. In order to facilitate the comparison of the influence of the salinity of the well fluid on the measurement, a rectangular coordinate system is established with the center of the circular damage, the abscissa is the radius of the circular damage, and the ordinate is the equivalent resistance between the detection electrode and the damage. Fig. 5(b) shows the numerical simulation results. The curve shows: (1) In the well fluid environment with the same salinity, the equivalent resistance value decreases rapidly with the increase of the radius r_a of the damaged part, until it remains at a relatively stable value; (2) The salinity parameters have a great influence on measured resistance, so it is necessary to conduct salinity calibration experiments in the future. (3) In the condition of the same damage radius, the equivalent resistance value decreases with the increase of the salinity of the well fluid and vice versa.

Gang G and others have done similar research work [39]. By fitting the experimental data, they obtained the fitting relationship between the equivalent resistance R_x and the damage radius r_a as $R = a \cdot r_a^b$, both a and b are constants. Refer to its index relationship, Referring to its exponential relationship, we try to fit the data obtained from simulation calculation and get the result under the default salinity of 0.1 ms/cm.

$$R_x = 1913 {r_a}^{-0.8717} + 326.55 \tag{17}$$

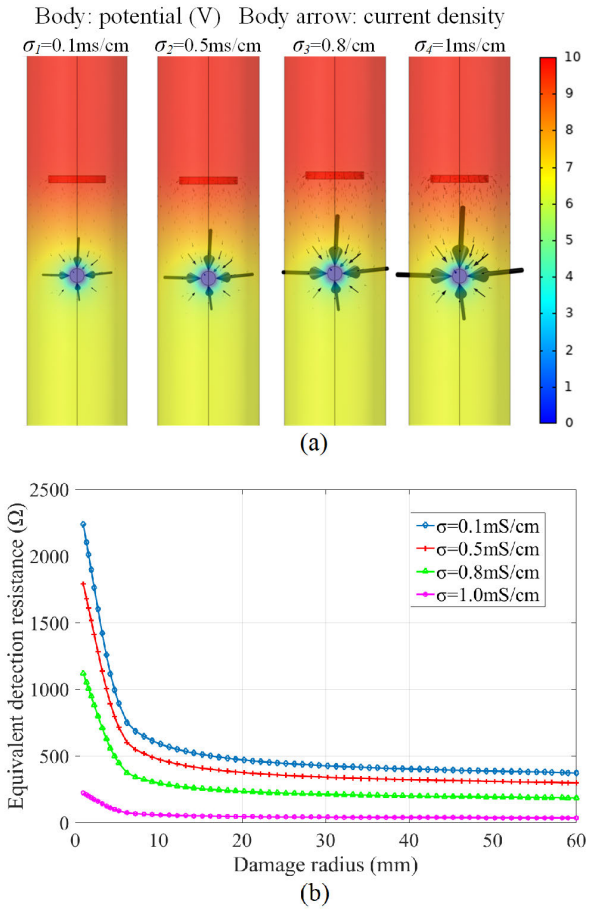

FIGURE 5. Schematic diagram of potential distribution in casing. (a) Current density and potential distribution under different salinity; (b)Equivalent impedance at different salinity.

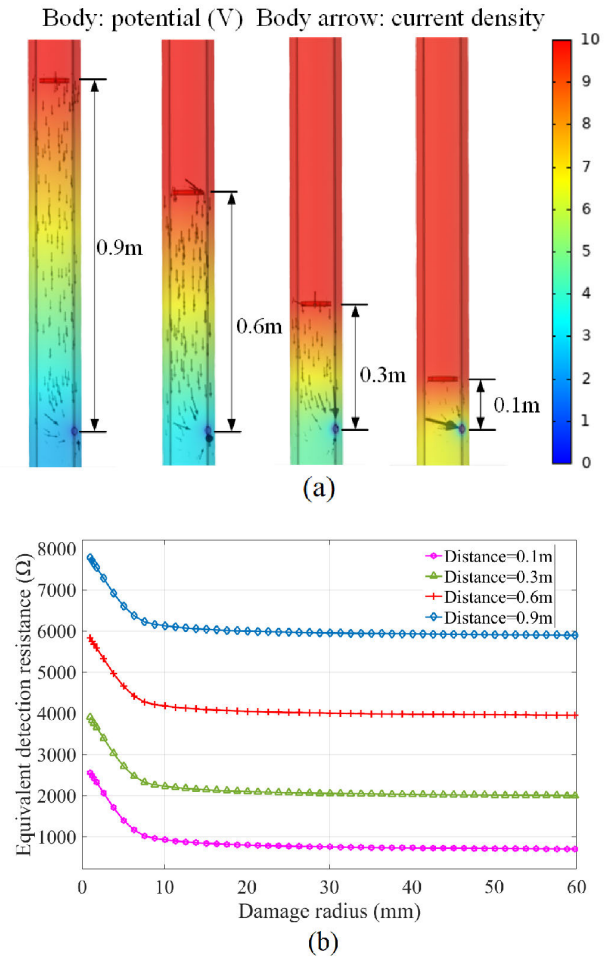

FIGURE 6. The relationship between electrode distance and equivalent impedance. (a) Potential distribution and current density at different distances; (b) Simulation results at different electrode distances.

Equation (17) has good goodness of fit ($R^2 = 0.999$), which shows that there is an exponential function relationship between the equivalent resistance value and the damage radius in the model, which is mutually verified with other research conclusions.

2) THE INFLUENCE LAW OF ELECTRODE POSITION, SIZE AND DAMAGED AREA

To study the influence of the distance between the detection electrode and the damaged point on the measurement results, four different distance conditions were chosen for simulation, and the calculation results are shown in Fig. 6. Fig. 6(a) shows that there is a significant change in potential during the detection. The current density per unit volume increases as the distance decreases. The curve in Fig. 6(b) shows: (1) When the damage radius is in the range of 0 to 10mm, R_x drops rapidly from the maximum value; (2) With the increase of the damage radius, the descending speed of R_x obviously slows down, and gradually approaching a resistance value which is highly related to the damage distance of the electrode; (3) When the damage radius is the same, there is an approximately linear relationship between R_x and the electrode spacing, and the damage position of the coating can be calculated quantitatively by R_x.

To further explore the influence of the size and damaged area of the detection electrode on R_x, we combined the parameters r_a and h_b in the model to carry out a joint scanning calculation and got the simulation results as shown in Fig. 7. The curved surface in Fig. 7 shows that: in the case that the radius of the detection electrode remains unchanged, the width h_b of the detection electrode has little influence on impedance measurement. Considering that the skeleton of the instrument needs a certain strength in actual downhole operation, the outer radius of the detection electrode should be consistent with that of the instrument.

3) DISTRIBUTION SCHEME OF SHAFT AXIAL DETECTION ELECTRODE

The simulation results in the previous section show that when the damaged area is large, the impedance change rate obtained by using a single detection electrode is very small. To obtain higher axial resolution, we propose an axial double-electrode rings detection scheme. In the following,

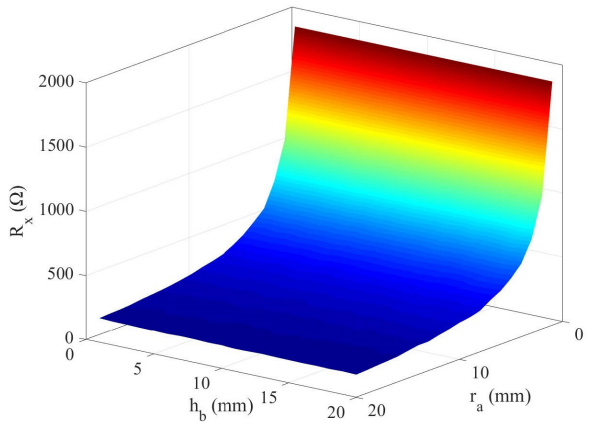

FIGURE 7. The influence of electrode width and damage radius on the measured resistance.

the single and double-detection electrode rings are simulated respectively, and the simulation results shown in Fig. 8(a) are obtained. The results in the figure show that: in the case of a single-electrode ring, the current is prone to escape, which is not conducive to the current collection. When the double-electrode rings solution is adopted, the electric potential of the damaged part in the casing changes obviously, and the current trend is more concentrated, which is beneficial to improve the longitudinal resolution of the damaged part.

The curve in Fig. 8(b) and Fig. 8(c) shows that: (1) When the damaged point and the electrode are at the same depth (the abscissa is 0), the curve of equivalent impedance is a minimum value at this point, which further shows that the ring-shaped detection electrode can locate the damaged position. (2) It is verified that there is an approximately linear relationship between the equivalent resistance and the electrode distance. (3) Compared with the single-ring electrode, the change rate of equivalent impedance after using the double-ring electrode is significantly increased, regardless of single-point damage or multi-point damage(k1>k3, k2>k3), from the highest 655Ω/m to 8000 Ω/m. It is equivalent to further increasing the variation range of the equivalent impedance to be measured, which is conducive to improving the detection dynamics and measurement accuracy of the instrument. Therefore, it is advisable to use a double-electrode ring to complete the depth location and area estimation of the damage.

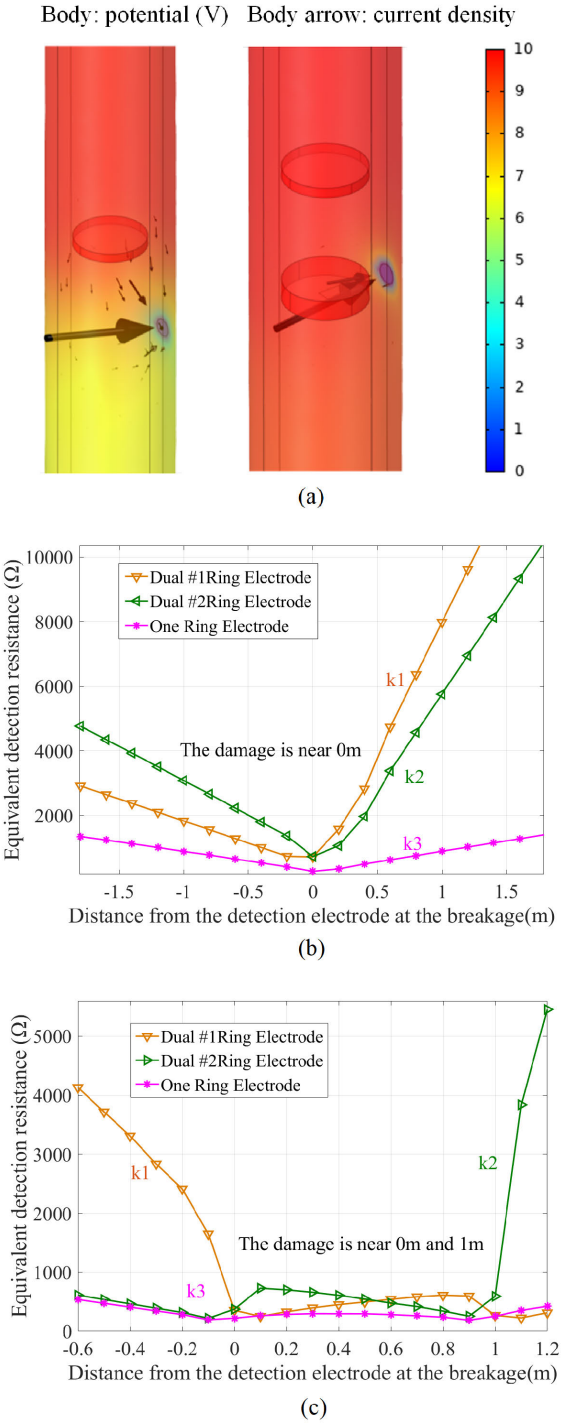

FIGURE 8. The influence of the number of electrodes and damage radius on resistance measurement. (a) Potential Distribution and Current Density of Single and Double Electrode Ring; (b) Simulation results of a single damage part; (c) Simulation results of two damaged parts.

4) DISTRIBUTION SCHEME OF RADIAL DETECTION ELECTRODES IN WELLBORE

Although the electrode ring can effectively identify the location of the axial damage point in the wellbore, this structure can not identify the specific location of the radial damage point in the round wellbore. To this end, we propose a radial four-arm electrode detection scheme, and its structure is shown in Fig. 9(a). The arm electrodes are supported by a spring, and under the action of tensile force, four point-shaped detection electrodes are pushed to the vicinity of the inner wall of the wellbore. The four-arm electrodes at the same depth as the wellbore divide the wellbore into four quadrants radially. The polar coordinate system is established with the center of the wellbore as the origin and the radius of the wellbore as the radius. Assuming that #1 Arm electrode is

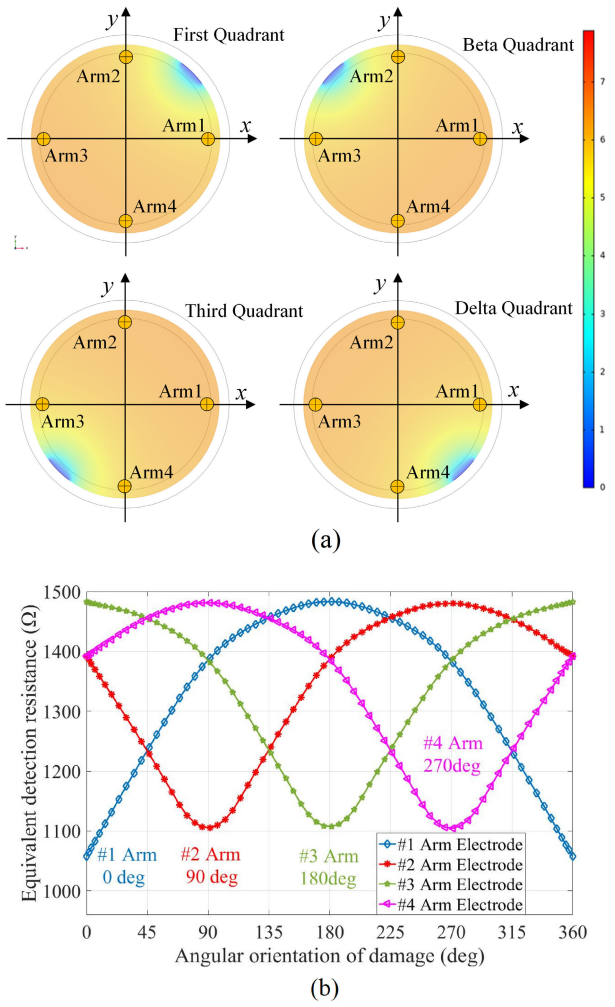

FIGURE 9. Simulation results of spot detection electrode.(a) The potential distribution of the damage in different quadrants; (b) Simulation results with different polar angles.

located at the polar angle of 0°, #2 Arm to #4 Arm electrodes are located at polar angles of 90°, 180°, and 270°, respectively. When the damage points appear in the 4 quadrants in sequence, the electric field distribution in the wellbore is simulated, and the result is shown in Fig. 9(a). The simulation results show that the electric field near the damaged area changes significantly, and the radial orientation of the damaged area can be determined by using 4 arm electrodes.

The simulation curves in Fig. 9(b) show that: When the damage is located at the pole angle of 0°, the #1 Arm electrode is closest to the damage of the inner coating of the casing, where the equivalent resistance value is the smallest. The #3 Arm electrode is the farthest away from the damage, so its equivalent resistance is the largest. Because the radial distance between the #2 Arm electrode and the #4 Arm electrode and the damaged part is equal, their equivalent resistance values remain the same. In the same way, it can be found that when the polar angle of the damage is at 90°, the equivalent resistance of #2 Arm electrode is the smallest. We can see that the detection resistance curve changes symmetrically within

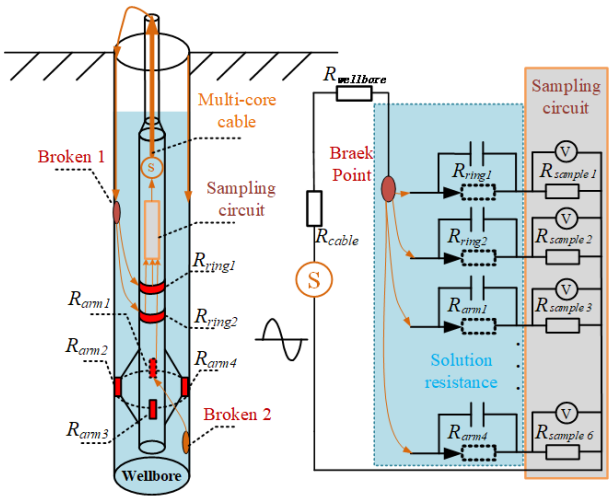

FIGURE 10. Schematic diagram of casing coating damage detection scheme.

the polar angle range. Therefore, by comparing the equivalent impedance of the four arm electrodes, the radial orientation of the damage can be judged. In summary, the following simulation conclusions can be obtained. (1) The circuit that detects the current needs to be isolated. (2) Designing a double electrode ring can effectively improve the axial positioning accuracy of the damaged point. (3) The use of four-arm electrodes can realize the radial positioning of the damaged position.

5) DETECTING SCHEME DESIGN

The detection principle of casing inner coating damage is shown in Fig. 10. Two electrode rings named E_{ring1} and E_{ring2} are installed at the upper end of the cylindrical instrument, and four arm electrodes named E_{arm1} to E_{arm4} are installed at the lower end of the instrument. A circuit board is placed in the instrument, which is mainly used for providing excitation voltage and sampling current on multi-electrode channels. Among them, the excitation voltage source is named S, and one end of it is connected with a cable core in the underground multi-core cable. Hereinafter named as communication cable. Use the communication cable to send the current to the ground and connect with the ground end of the metal casing. If a sampling resistor $R_{\text{sample x}}$ is connected in series between each electrode and S, the current of each sampling channel can be calculated by measuring the voltage on each sampling resistor. This current is inversely proportional to the sum of the well fluid impedance formed between each electrode (R_{ring1} to R_{ring4}) and the damaged point, the wellbore resistance R_{wellbore} and the resistance R_{cable} of the communication cable. Because the resistance of wellbore and the resistance of communication cable are relatively fixed, the above method can indirectly calculate R_{ring1} to R_{arm4}. Because the well fluid impedance is closely related to the damage position of the electrode and the inner coating, the corresponding damage position of the casing inner coating can also be found.

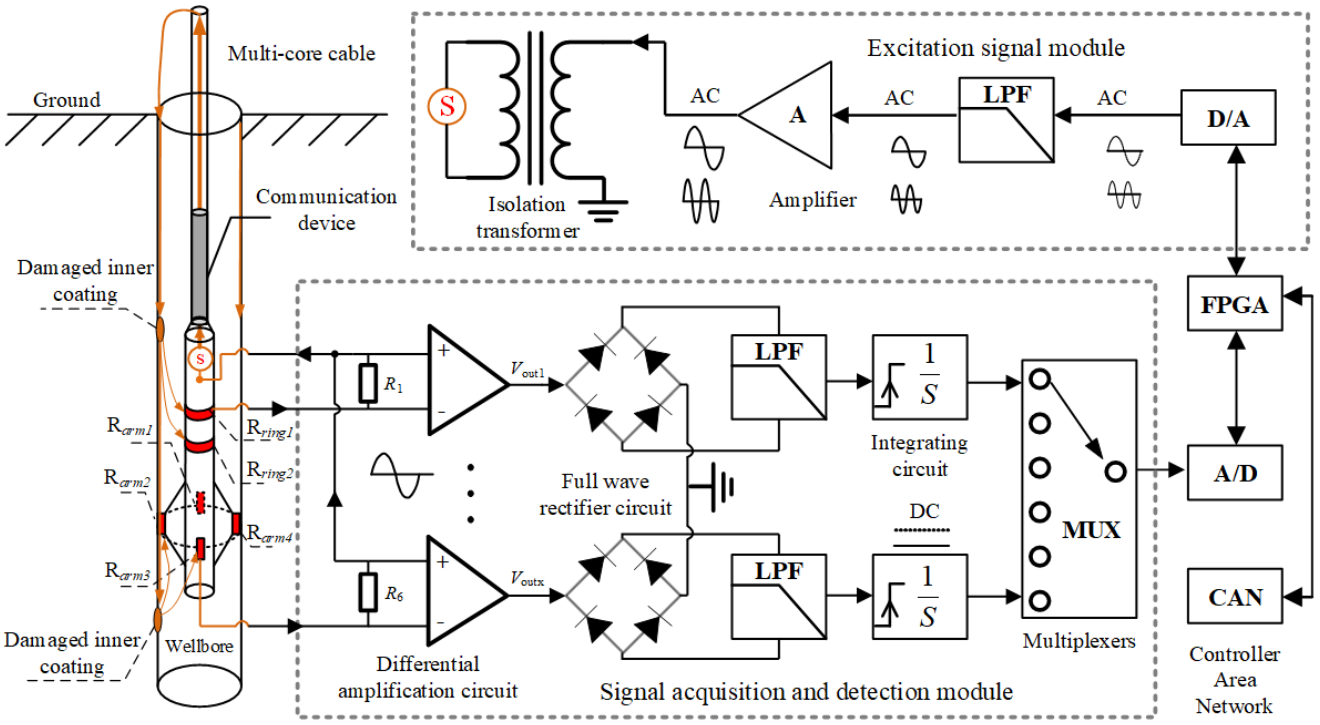

FIGURE 11. Schematic diagram of the overall design of the instrument.

III. INSTRUMENT SYSTEM SCHEME

A. INSTRUMENT SYSTEM DESIGN

According to the above detection scheme, the overall schematic design of the instrument is designed as shown in Fig. 11, which is composed of the logic control module, generate stimulus signal module, the acquisition processing module, and communication module. Specific functions are described as follows: (1) Logic control module. To satisfy the real-time consideration of signal detection and data communication, the FPGA (Field Programmable Gate Array) is selected as the main control chip. (2) Generate stimulus signal module. The excitation module is mainly composed of a voltage source and signal isolation. Voltage source module includes FPGA, DA converter, and operational amplifier. The excitation source uses DDS(Direct Digital Synthesis) technology to generate sinusoidal signals with frequencies of 1KHz and 2KHz in time-sharing. After low-pass filtering and power amplification, the sinusoidal signal becomes an AC voltage signal with an offset of 0V and peak-to-peak value of 10V. Because the measured current loop is connected with the ground through the casing, the isolation transformer is used to isolate the ground between the two, which reduces the interference between the ground and the ground of the circuit board and realizes the current collection. The isolation transformer is wound with 84:84 turns to ensure that the input impedance of the primary side and the output impedance of the operational amplifier are as consistent as possible to obtain the maximum transmission power. (3) Acquisition processing module. To solve the problem that the equivalent resistance value of the detection electrode is infinite when there is no current loop formed, the anti-open circuit resistance is connected in parallel at both ends of the equivalent resistance value. According to Kirchhoff's voltage law, after the excitation signal passes through the impedance network, the AC voltage signal containing impedance information is obtained on the sampling resistor. Then, the voltage difference between the two ends of the sampling resistor is sampled and amplified by the instrumentation amplifier, and then the sampled signal is subjected to full-wave rectification and low-pass filtering, and the AC signal is converted into a unipolar voltage signal. On this basis, the signals are sent to the AD converter for analog-to-digital conversion by using a multiplexer, and the signal acquisition and processing are completed. (4) Communication module. To improve the efficiency of data transmission and reduce the interference of complex electrical noise in the well, the CAN (Controller Area Network) bus is used for communication between the instrument and the data acquisition box. After receiving the remote frame command from the data acquisition box, the casing inner coating inspection instrument performs normalization processing and data arrangement on the multi-channel measurement data, and communicates with the data acquisition box through the CAN bus.

B. DETECTING CIRCUIT BOARDS AND INSTRUMENTS

A detection circuit board manufactured according to the above detection scheme is shown in Fig. 12. Due to the space limitation of downhole tools, a design scheme of

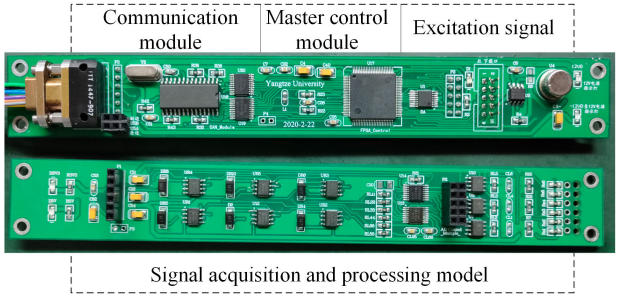

FIGURE 12. Detecting circuit boards.

two circuit boards is adopted, and the circuit board size is 185mm*25mm. On the left side of the upper circuit board is the communication module, and the communication protocol is the CAN bus. The middle part of the upper circuit board is the main control module (FPGA), which is responsible for the logic control of the system. On the right side is the generate stimulus signal module, which is used to generate a stable sinusoidal excitation signal. The lower circuit board is responsible for the acquisition, processing, and analog-to-digital conversion of analog signals. Fig. 13 shows the actual picture of the detecting instrument. The instrument has through-cables, arm electrodes, ring electrodes, and instrument compartments from left to right. The left end of the instrument has a through-cable reserved inside, which can be conveniently connected to other instruments. The 4 arm electrodes are pushed against the inner wall of the casing through the ceramic support arm. The end of the support arm adopts a roller design to ensure that the arm electrodes effectively contact the inner wall of the casing while avoiding scratches on the inner coating. The radius of the two ring electrodes is consistent with the radius of the shell of the instrument, and the surface is concavo-convex to ensure full contact with the well fluid medium. All measuring electrodes are introduced into the instrument compartment inside the right end of the instrument through the insulating pressure-bearing sealing plug and connected with the detection circuit board.

IV. EXPERIMENTAL PROCESS AND DATA ANALYSIS

To test the performance of the instrument indoors and further optimize the detection parameters of the instrument, an experimental device as shown in Fig. 14 was designed. The experimental device uses a plexiglass cylinder to simulate the downhole casing. The detection instrument for the inner coating of the casing is placed in the cylinder, and the detection instrument communicates with the computer through a cable and a data acquisition box. To simulate the damage with different damage radii, one end of the cable is connected to the mouth of the metal sleeve, and the other end is connected with a metal disc with a known radius. The metal disc is attached to the inner wall of the cylinder to simulate the damage of the inner coating.

In order to explore the relationship between sampling resistance and well fluids with different salinities, we selected an appropriate sampling resistance and carried out a salinity

TABLE 2. Equivalent resistance under different brine concentrations.

	Resistance values at different brine concentrations				
Detection electrode	0g/L	1g/L	10g/L	50g/L	120g/L
#1Ring	24920Ω	3632Ω	1339Ω	857Ω	591Ω
#2Ring	23837Ω	3400Ω	1405Ω	914Ω	643Ω
#1Arm	22921Ω	3514Ω	1405Ω	857Ω	643Ω
#2Arm	22920Ω	3400Ω	1339Ω	857Ω	643Ω
#3Arm	22657Ω	3400Ω	1339Ω	858Ω	617Ω
#4Arm	22920Ω	3632Ω	1339Ω	857Ω	591Ω

TABLE 3. Differential voltage of different sampling resistors.

	Partial voltage value of sampling resistance at different salinity				
Rsample	25KΩ	12KΩ	1KΩ	100Ω	Range
100Ω	0.11V	0.21V	2.1V	6.94V	6.83V
200Ω	0.22V	0.43V	3.91V	7.47V	7.25V
330Ω	0.33V	0.64V	5.47V	7.64V	7.31V
400Ω	0.44V	0.85V	6.43V	7.73V	7.29V
500Ω	0.55V	1.05V	6.75V	7.78V	7.23V
600Ω	0.66V	1.26V	6.95V	7.82V	7.16V
700Ω	0.77V	1.46V	7.09V	7.84V	7.07V
1KΩ	1.09V	2.04V	7.38V	7.89V	6.8V
3KΩ	3.03V	5.32V	7.78V	7.95V	4.92V

experiment. The experiment simulates the well fluid environment of different salinity, adding water into the casing, and then adding quantitative NaCl in batches. The equivalent impedance of solutions with different salinity was measured, and the experimental results are shown in Table 2.

It can be seen from the data in Table 2 that the resistance of the solution varies from 25KΩ to several hundred ohms in the experiment. According to Kirchhoff's voltage law. When the solution resistance is between 100 Ω and 25 KΩ, the voltage difference between the two ends of the sampling resistor is calculated when different resistance values are selected. The calculation results are shown in Table 3.

By comparing the voltage dynamic range of the sampling resistor in Table 3, it can be seen that the optimal value of the sampling resistor is 330Ω. The AD conversion precision of the detection circuit is 16 bit, and the theoretical detection performance is as high as 93 dB, which ensures that the instrument still has high resolution under different salinity well conditions. To verify the detection accuracy of the designed two detection electrode rings and four arm electrodes, an experiment was carried out to locate the damaged part of the casing inner coating. In the experiment, the controlled variable method is used to simulate the well fluid environment with different salinity by changing the NaCl content in water. The distance between the #3 Arm electrode of the control instrument and the damaged part is the closest, and record the equivalent resistance of each measuring electrode and the damaged part. The experimental results are shown in Fig. 15.

The curve in Fig. 15 shows that: (1) Under the environment of high salinity, the equivalent resistance of the instrument will decrease obviously. (2) The equivalent resistance value detected by the instrument #3 electrode is obviously different from other channels because the #3 electrode is closest to the

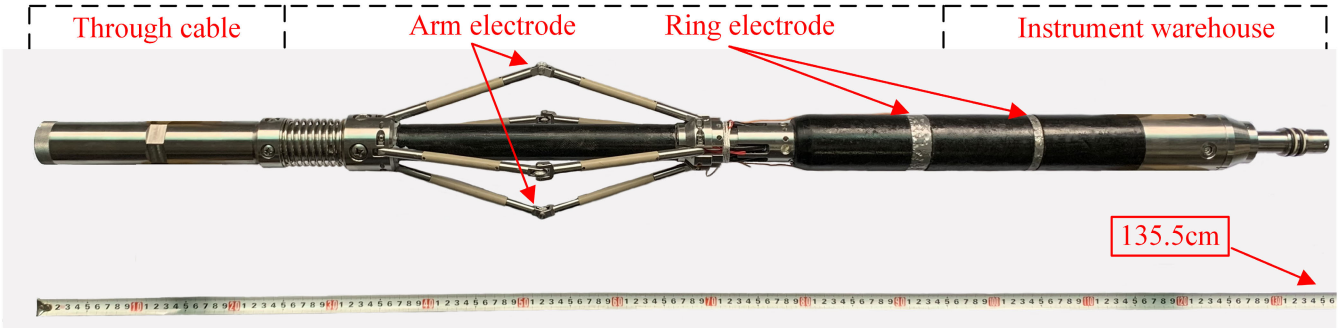

FIGURE 13. Schematic diagram of the overall design of the instrument.

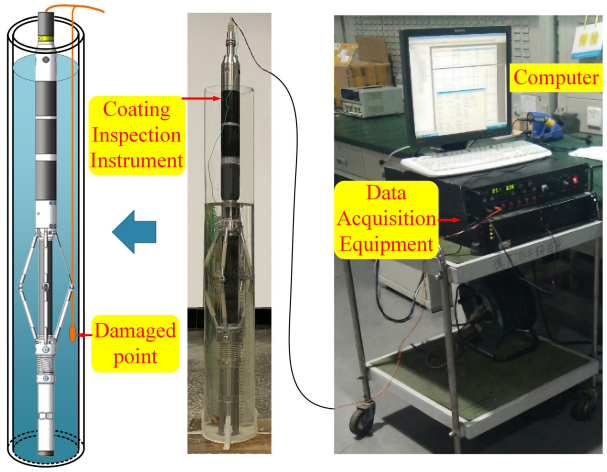

FIGURE 14. Instrumentation and experimental setup.

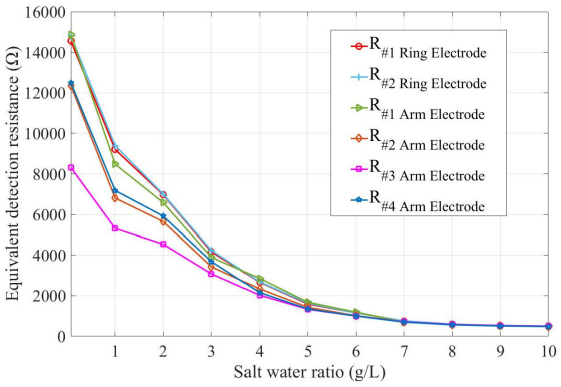

FIGURE 15. Test results under different salinity.

damaged position, which can accurately locate the damaged position, which is consistent with our expectation. (3) The instrument has good resolution and sensitivity in low salinity. With the increase of salinity, the equivalent resistance values of the six electrodes are gradually approaching, and the resolution of the instrument detection can be further improved.

V. FIELD TEST RESULTS AND DATA ANALYSIS

The inner coating detector of the downhole casing uses four measuring arm electrodes and two ring electrodes as a combined sensor to measure. The maximum opening

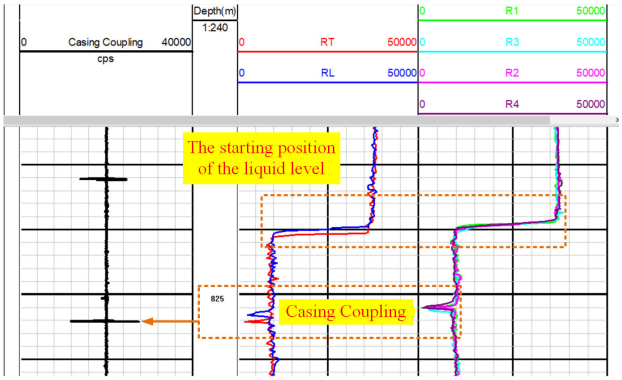

FIGURE 16. Field test results of casing inner coating 1.

diameter of the four-arm electrode is 152mm, which can effectively stick to the casing diameter of 5.5 inches. The logging software adopts a production logging ground system independently developed by CNPC (China National Petroleum Corporation) logging. The inner coating inspection instrument of the casing is connected to the platform in the form of a function library. The inner coating inspection instrument of the casing is connected to the platform in the form of a function library. During field logging, the casing internal coating detector and the four-parameter telemetry communication instrument are used to go down the well. Therefore, in actual logging, not only six coating resistivity curves can be obtained, but also parameters such as gamma, well temperature, pressure, and magnetic coupling can be obtained, which provides a reliable basis for the calibration and verification of coating instruments. Six detection electrode curves in integrated acquisition software are as follows, RT(#1 Ring electrode); RL(#2 Ring electrode), R1, R2, R3, and R4 correspond to four arm electrodes(#1 Arm electrode to #4 Arm electrode). The actual logging results in well pad Shang 60-591 are shown in Fig. 16 and Fig. 17.

The results in Fig. 16 show that the equivalent resistances of the six detection channels are all maximum values before the instrument reaches the downhole liquid level. After the detection electrode of the instrument comes into contact with the well fluid, the excitation signal source forms a detection current loop through the well fluid. At this time, the equivalent resistance decreases rapidly due to a certain salinity in the

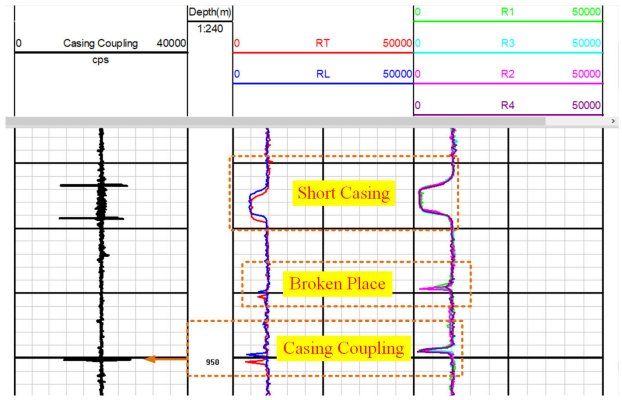

FIGURE 17. Field test results of casing inner coating 2.

well fluid. Not all downhole casings are covered with coatings, and the coupling part between the casings is bare, so the instrument also has a response curve to casing coupling.

The curve results in Fig. 17 show that when the instrument detects the uncoated short casing, the equivalent resistance values of the six detection electrodes all show an obvious downward trend, which shows that the instrument responds quickly to the uncoated casing. When the inner coating is damaged at a certain depth of the casing, the equivalent resistance of the RT and RL electrodes will show a downward trend. By observing the curve, we can see that the equivalent resistance of R2 decreases significantly. Therefore, it can be judged that the inner coating near the R2 electrode is damaged at this depth. In summary, the casing inner coating inspection instrument is a very effective means of evaluating the quality of the casing inner coating in new wells and the integrity appraisal of the casing coating in old wells.

VI. CONCLUSION

In this paper, according to the detection requirements of the inner coating damage of downhole casing, we explained the basic principle of the conductivity method to measure the quality of the inner coating of the casing, analyzed four conductivity measurement methods, and discussed the key issues of conductivity detection. On this basis, the influence of well fluid salinity was analyzed through numerical simulation. Besides, the arrangement scheme of the axial two-ring electrode and the radial four-wall electrode was put forward, and the detection circuit of the dual-frequency signal source was designed. Experiments were carried out indoors and outdoors, and the experimental results show that the prototype can work reliably under the well condition with salinity lower than 120g/L, which provides an effective detection method for the quality evaluation of casing inner coating.

REFERENCES

[1] S. Dai, T. Zhang, S. Mo, Y. Cai, W. Yuan, T. Ma, L. Hu, and B. Wang, "Study on preparation, thermal conductivity, and electrical insulation properties of epoxy/AlN," *IEEE Trans. Appl. Supercond.*, vol. 29, no. 2, pp. 1–6, Mar. 2019.

[2] J. Wang, Z. Y. Bi, J. N. Zhang, Y. Wang, C. Li, H. Bai, S. L. He, and T. Wang, "Current situation of oil casing corrosion and protection technology," *Welded Pipe*, vol. 36, no. 7, pp. 57–62, 2013.

[3] Y. Pan, L. Sun, S. C. Yang, and B. Yu, "Research progress of pipeline corrosion and protection at home and abroad," *Corrosion Sci. Protection Technol.*, vol. 26, no. 1, pp. 77–80, 2014.

[4] Z. Y. Xue, W. X. Bi, Z. H. Chen, F. Zhang, and H. Y. Chen, "Current situation and prospect of oil and gas pipeline cathodic protection technology," *Oil Gas Storage Transp.*, vol. 33, no. 9, pp. 938–944, 2014.

[5] J. Huang, "Current status and prospects of cathodic protection technology of oil and gas pipeline," *Petrochem. Ind. Technol.*, vol. 24, no. 9, p. 83, 2017.

[6] L. Y. Xu and Y. F. Cheng, "Reliability and failure pressure prediction of various grades of pipeline steel in the presence of corrosion defects and pre-strain," *Int. J. Pressure Vessels Piping*, vol. 89, pp. 75–84, Jan. 2012.

[7] Z. C. Qiu, C. M. Xiong, Z. L. Chang, Z. H. Zhao, C. Zhao, and Z. R. Ye, "The application of phase technology of tubing inner coating in Tazhong no. 1 gas field," *Natural Gas Ind.*, vol. 32, no. 10, pp. 128–129, 2012.

[8] Q. Wang, "Application of electromagnetic thickness logging technology in Iranian Oilfield," *Chem. Anagement*, vol. 4, no. 6, pp. 128–129, 2020.

[9] J. Sun, "Analysis of factors affecting measurement accuracy of multi-arm caliper," *China Petroleum Chem. Standards Qual.*, vol. 37, no. 22, pp. 41–42, 2017.

[10] Y. Yang, H. Liu, Q. He, H. J. Li, and H. X. Chen, "Experimental analysis of ultrasonic imaging logging tool in calibration well group," *Petroleum Tubing Instrum.*, vol. 5, no. 1, pp. 75–79, 2019.

[11] X. Z. Zhang, L. H. Yang, Q. W. Li, J. J. Qi, B. H. Cheng, H. Y. Yuan, C. L. Fu, and X. Y. Wang, "A quality detection device and detection method for downhole casing inner coating," Chinese and Foreign Patent 201 810 266 483.8, Mar. 28, 2018.

[12] Q. W. Li, B. H. Cheng, Z. W. Tang, J. Q. Xue, C. L. Fu, H. L. Yang, Z. W. He, L. H. Yang, Z. X. Zhang, and Y. L. Sun, "A single-electrode current detection method for the inner coating of downhole tubing and casing," Chinese and Foreign Patent 201 510 621 431.4, Sep. 25, 2015.

[13] B. H. Cheng, J. Q. Xue, Q. W. Li, X. Z. Zhang, H. L. Yang, Y. Jiang, Y. L. Sun, W. Liu, C. L. Fu, H. Y. Yuan, and P. Zhou, "A three-electrode potential difference detection method for the inner coating of downhole tubing and casing," Chinese and Foreign Patent 105 239 995.A, Jan. 13, 2016.

[14] X. Deng, H. Gu, L. Yang, H. Lyu, Y. Cheng, L. Pan, Z. Fu, L. Cui, and L. Zhang, "A method of electrical conductivity compensation in a low-cost soil moisture sensing measurement based on capacitance," *Measurement*, vol. 150, Jan. 2020, Art. no. 107052.

[15] Z. J. Wan, J. B. Liao, Y. K. Wang, and G. F. Yin, "Research on metal pipeline pit corrosion monitoring based on potential array," *Chin. J. Sci. Instrum.*, vol. 32, no. 1, pp. 19–25, 2011.

[16] Y. C. Wu, J. T. Zhang, and Z. G. Yan, "Research on AC impedance detection and location method of casing defects," *J. Xi'an Shiyou Univ., Natural Sci. Ed.*, vol. 30, no. 6, pp. 101–107, 2015.

[17] G. S. Li, Y. Zhao, and Y. F. Lu, "Application of casing inner coating detector in changqing oilfield casing coating detection," in *Proc. IFEDC*, Xi'an, China, 2018, pp. 2901–2907.

[18] A. Samimi and S. Zarinabadi, "Application polyurethane as coating in oil and gas pipelines," *Int. J. Sci. Investigations*, vol. 1, no. 8, pp. 43–45, 2012.

[19] P. K. Shukla, A. Nordquist, and F. Song, "Development of cased-pipeline corrosion model and its validation with experimental data," in *Proc. CORROSION*. San Antonio, TX, USA: OnePetro, 2014, pp. 43–53.

[20] E. Popek, *Sampling & Analysis of Environmental Chemical Pollutants. A Complete Guide*. New York, NY, USA: Academic, 2003.

[21] X. Shi, C. Tan, F. Dong, E. N. dos Santos, and M. J. da Silva, "Conductance sensors for multiphase flow measurement: A review," *IEEE Sensors J.*, vol. 32, no. 10, pp. 128–129, Jun. 2012.

[22] Z. C. Qiu, C. M. Xiong, Z. L. Chang, Z. H. Zhao, C. Zhao, and Z. R. Ye, "The application of anti-corrosion technology of tubing inner coating in Tazhong no. 1 gas field," *Natural Gas Ind.*, vol. 32, no. 10, pp. 86–89, 2012.

[23] M. Feng, "Array type resistance water holdup detection method and instrument research," Yangtze Univ., Jingzhou, China, Tech. Rep. 12, 2018.

[24] H. J. Lin, S. H. Li, L. C. Wang, and G. F. Liu, "A fast identification method of doped coal based on AC impedance," *J. Electron. Meas. Instrum.*, vol. 29, no. 4, pp. 577–583, 2015.

[25] L. Su, X. Liao, and Z. Huang, "A theoretical study on resistance of electrolytic solution: Measurement of electrolytic conductivity," *Results Phys.*, vol. 13, Jun. 2019, Art. no. 102274.

[26] D. Wang, N. Jin, L. Zhai, and Y. Ren, "Salinity independent flow measurement of vertical upward gas-liquid flows in a small pipe using conductance method," *Sensors*, vol. 20, no. 18, p. 5263, Sep. 2020.

[27] C. Q. Zhong, J. H. Lan, and S. Y. Yang, "A resistance measurement method to eliminate the influence of distributed capacitance," *J. Dalian Univ. Technol.*, vol. 43, no. 3, pp. 372–376, 2003.
[28] B. Y. Li and C. Zhao, "Design and implementation of broadband AC impedance test system," *Instrum. Technol. Sensor*, vol. 3, no. 3, pp. 82–85, 2018.
[29] S. C. Gao, "Design of a dual-frequency sinusoidal signal conductivity measuring instrument," Dalian Univ. Technol., Dalian, China, Tech. Rep. 6, 2010.
[30] S. Malik, K. Kishore, T. Islam, Z. H. Zargar, and S. Akbar, "A time domain bridge-based impedance measurement technique for wide-range lossy capacitive sensors," *Sens. Actuators A, Phys.*, vol. 234, pp. 248–262, Oct. 2015.
[31] D.-H. Kim, M. Chauhan, M.-O. Kim, W. C. Jeong, H. J. Kim, I. Serša, O. I. Kwon, and E. J. Woo, "Frequency-dependent conductivity contrast for tissue characterization using a dual-frequency range conductivity mapping magnetic resonance method," *IEEE Trans. Med. Imag.*, vol. 34, no. 2, pp. 507–513, Feb. 2015.
[32] Z. Lin, X. Zhang, J. L. Wei, X. P. Wang, and X. Yu, "Absolute measurement method of solution conductivity based on vanderbilt method," *Acta Metrol.*, vol. 36, no. 2, pp. 176–180, 2015.
[33] D. L. Corwin and K. Yemoto, "Salinity: Electrical conductivity and total dissolved solids," *Soil Sci. Soc. Amer. J.*, vol. 84, no. 5, pp. 1442–1461, Sep. 2020.
[34] K. D. C. Cunha, L. D. S. Pardellas, and F. B. Gonzaga, "Stability monitoring of electrolytic conductivity reference materials under repeated use conditions by the primary measurement method," *J. Solution Chem.*, vol. 49, no. 3, pp. 306–315, Mar. 2020.
[35] D. Vasic, V. Bilas, and A. J. Peyton, "Induction conductivity measurement of surrounding low-conductive medium from copper tube-experimental verification," in *Proc. IEEE Int. Instrum. Meas. Technol. Conf.*, May 2012, pp. 314–317.
[36] Z. N. Xu, F. C. Lv, H. M. Li, and Y. P. Liu, "Influencing factors and optimization of insulator electric field finite element analysis method," *High Voltage Technol.*, vol. 37, no. 4, pp. 944–951, 2011.
[37] Y. Wei, H. Yu, Q. Chen, G. Liu, C. Qi, and J. Chen, "A novel conical spiral transmission line sensor-array water holdup detection tool achieving full scale and low error measurement," *Sensors*, vol. 19, no. 19, p. 4140, Sep. 2019.
[38] S. Wang, J. L. Corredor Garcia, J. Davidson, and A. Nichols, "Conductance-based interface detection for multi-phase pipe flow," *Sensors*, vol. 20, no. 20, p. 5854, Oct. 2020.
[39] G. Guo, Q. Li, B. Cheng, W. Lu, L. Yang, and Z. Zhou, "Electrode tool logging approaches for casing inner coating monitoring," in *Proc. NACE Int. Corrosion Conf.*, 2020, pp. 1–9.

TAO GUO received the B.S. degree in electrical and information engineering from Yangtze University, Jingzhou, China, in 2015, where he is currently pursuing the M.S. degree in communication and information systems.

His research interests include process parameter detection, down-hole petroleum instrumentation, and signal analysis.

YONG WEI received the B.S. degree in electrical and information engineering from the Jianghan Petroleum Institute, China, in 2003, and the M.S. degree in signal and information processing and the Ph.D. degree in geodetection and information technology from Yangtze University, Jingzhou, China, in 2006 and 2016, respectively.

He was with the Department of Automation, Yangtze University, as a Lecturer, from September 2006 to August 2016. Since 2016, he has been an Associate Professor with the Department of Measurement and Control Technology and Instrumentation, Yangtze University. From October 2018 to October 2019, he was a Visiting Scholar with the University of Houston, Houston, TX, USA. His main research interests include new method and instrument for acoustic and electric well logging.

KE LI received the B.S. degree in electronic instrument and measurement technology from the Jianghan Petroleum Institute, China, in 2000, and the M.S. degree in instrumentation from Xi'an Petroleum University, Xi'an, China, in 2013.

He was with the Technology Center, China Petroleum Logging Company Ltd., engaged in the development of radiological and electrical instruments, from 2003 to 2015. Since 2016, he has been working with the Production Logging Center, China Petroleum Logging Company Ltd., engaged in the development of engineering logging, residual oil monitoring, and other logging instruments.

QIANG CHEN received the B.S. degree in electronic information science and technology from Heze University, China, in 2010, and the M.S. degree in electronic and communication engineering from Yangtze University, Jingzhou, China, in 2012.

He was with the Technology Center, China Petroleum Logging Company Ltd., as an Assistant Engineer, from July 2012 to June 2015. Since 2016, he has been an Engineer with the Production Logging Center, China Petroleum Logging Company Ltd. His research interests include logging tools for water injection and production fluid profile.

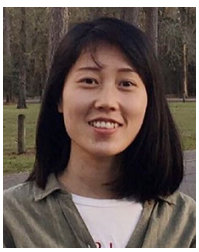

LI YAN received the B.S. degree in electronic engineering from the University of Electronic Science and Technology of China, Chengdu, China, in 2016. She is currently pursuing the Ph.D. degree with the Department of Electrical and Computer Engineering, University of Houston, Houston, TX, USA.

Her research interest includes inverse problem for well logging applications in complex formation environments.

JIEFU CHEN (Senior Member, IEEE) received the B.S. degree in engineering mechanics and the M.S. degree in dynamics and control from the Dalian University of Technology, Dalian, China, in 2003 and 2006, respectively, and the Ph.D. degree in electrical engineering from Duke University, Durham, NC, USA, in 2010.

He was with the Department of Electrical and Computer Engineering, Duke University, as a Research Assistant, from September 2007 to December 2010. He was a Scientist with the Advantage Research and Development Center, Weatherford International Ltd., Houston, TX, USA. Since 2011, he has been an Assistant Professor with the Department of Electrical and Computer Engineering, University of Houston, Houston. His research interests include multi-physics modeling and inversion, fast algorithms in electromagnetics and acoustics, electronic packaging, underground and underwater wireless communication, and well logging.